Pergamon

Int. J. Mach. Tools Manufact. Vol. 35, No. 5, pp. 673–688, 1995

0890–6955/95$9.50 + .00

A NUMERICAL INVESTIGATION INTO CUTTING FRONT MOBILITY IN CO_2 LASER CUTTING

P. Di Pietro†‡ and Y. L. Yao†

(*Received* 22 *December* 1993; *in final form* 6 *June* 1994)

Abstract—The technologically important case of reactive gas laser cutting is examined. A transient two-dimensional (2D) model is developed specifically to investigate the effect of various CNC velocity profiles on the resulting cutting front temperature. Co-ordinated motion systems must ramp up and down to their target speeds, and therefore such accelerations must be considered. In doing so, the dynamics of the cutting front cannot be neglected. The implication of this mobility is that a net acceleration will result in greater, more efficient beam coupling to the workpiece, whilst a net deceleration results in a reduction, with the transmitted power simply falling through the generated kerf. The presence of such a kerf is considered and nodal points within it became part of the convective environment. Boundary encroachment and bulk heating issues, due to workpiece geometry, are also studied for their effect on the front temperature. Results show that even under non-accelerating conditions, cutting front mobility plays a significant role in temperature determination. A non-linear velocity profile is also evaluated via an optimization strategy in order to stabilize cutting front temperatures. The motivation being that quality can therefore be assured for intricate workpieces, which inherently have pre-cut sections and boundaries. Results on front mobility and temperature show similar trends as experimental and numerical results found elsewhere, whilst their direct verification is currently under investigation. Due to the hostile environment encountered in the interaction zone, the observation of such phenomena is extremely difficult.

NOMENCLATURE

A	area
A_b	absorptivity
a	net acceleration magnitude
amu	atomic mass units
b	kerf width
Bi	mesh-size Biot number
c_v	heat capacity
D	workpiece thickness
d	duct diameter
H	net energy input
h_c	mixed convective heat transfer coefficient
h_f	forced convective heat transfer coefficient
h_n	natural or free convective heat transfer coefficient
h_r	radiative heat transfer coefficient
$I(r)$	radial intensity distribution
$I(0)$	peak intensity
K	thermal conductivity
L	workpiece length
L_f	latent heat of fusion
$\dot{m}$	melt removal rate
n	outward normal co-ordinate
Nu_d	Nusselt number
$P_b(r)$	radial absorbed beam power
P_{exo}	exothermic power
P_{inc}	incident beam power
P_{melt}	melting power
P_{trans}	transmitted power
Pr	Prandtl number
$\dot{q}$	heat generation
q_r	radiative heat loss
r	radial distance from beam centre
ratio	ratio of FeO:Fe

†School of Mechanical and Manufacturing Engineering, The University of New South Wales, P.O. Box 1, Kensington, NSW 2033, Australia.
‡Author to whom all correspondence should be addressed.

R_b	laser beam radius
Re_d	Reynolds number
r_f	reflectivity
S	molten layer thickness
T	temperature
T_{melt}	melting temperature
t	time
V_b	velocity of laser beam
V_f	velocity of cutting front
W	workpiece width
x, y, z	co-ordinate axes
Y_b	laser beam position
Y_d	initial drilling position

Superscripts and subscripts

b	boundary point
f	front location
j	current time
m	nodal point in y direction
n	nodal point in x direction
o	initial value
∞	ambient conditions

Greek letters

α	thermal diffusivity
∂T	temperature tolerance
ΔH	exothermic energy release
ΔS	change in molten layer thickness from previous location
ΔS_b	distance beam has moved from its previous location
ΔS_f	distance front has moved from its previous location
Δt	timestep of integration
Δt_{inc}	fractional timestep of integration
$\Delta y = \Delta x$	spatial increments
ϵ	emissivity
σ_b	Stefan–Boltzmann constant
σ	mesh Fourier number
ρ	density
μ_m	mixed-mean coefficient of viscosity
μ_w	wall coefficient of viscosity

1. INTRODUCTION

MOST laser cutting applications today are of the two-dimensional (2D) contour type. Efforts in laser cutting research have so far concentrated almost exclusively on the simple case of linear constant velocity cutting. Admittedly, this is an appropriate area to investigate initially, but greater efforts are now needed to investigate more complex areas of concern. As we move from the realm of one-dimensional (1D) processing to two or more dimensional processing, we need to consider non-linear effects such as the dynamics of the handling system. With quality and productivity being of the utmost importance in today's economic climate, laser cutting cannot be perceived as simply a laser source, but needs to be considered as an overall system. CNC systems therefore need to be specifically tailored to the laser cutting industry, and at the very least, must develop at the same rate as the rest of the technology. A greater understanding of the effects of such controllers on the cutting process is therefore necessary.

In reality, co-ordinated motion systems must ramp up and down to desired target speeds in order to perform the part-programme generated. Refer to Fig. 1. In cases where applied heat fluxes are strong enough to melt the material though, the problem becomes complex due to the moving solid–liquid interface. Associated with this effect is the issue of non-linear beam coupling to the workpiece. Such accelerations will cause the cutting front to move at rates different from that of the beam. A net acceleration will mean that greater beam coupling will result as the beam will tend to ride ahead on the unmolten material. By analogy, a net deceleration will clearly result in greater inefficiency, as power will be lost through the kerf without any heating effect.

Even in the simple case of constant velocity cutting, the solid–liquid interface can move considerably and thus alter the energy input at the cutting front. The most

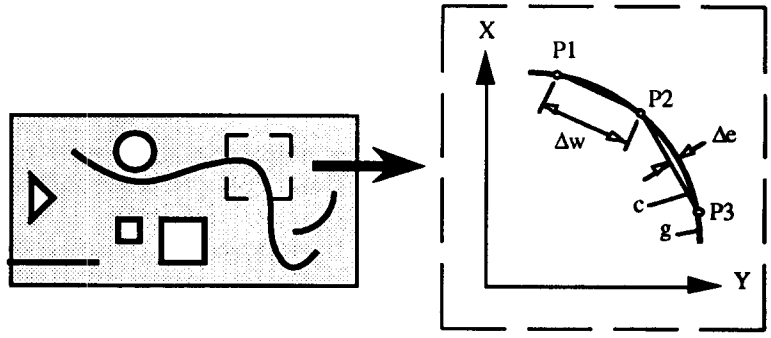

FIG. 1. Two-dimensional curvilinear machine-laser interpolation. P1, P2, P3, reference points; g, desired path; c, interpolation polygon; Δw, chordal length between reference points; x, y, co-ordinate axes; Δe, permissible tolerance between desired path and chord.

common assumption made in previous attempts at characterizing the process is that of infinite workpiece length [1]. Too often boundary conditions are trivialized by prescribing fixed boundary temperatures. Boundaries can be present in laser cutting in the form of workpiece edges or pre-cut sections, and are especially significant in laser cutting of intricate parts. Such simplifications allow the general heat conduction equation to revert to the case of steady multidimensional conduction where temperatures are invariant with time. It is obvious though that as the amount of heat accumulation to an area changes as in the case with a boundary encroachment, the cutting front can move significantly. Ideally for high quality cutting, the heat flux per unit time at the cutting front should always remain a constant. Any changes in this will be clearly observable by either increased dross attachment, roughness of cut or kerf widening.

Geometrical effects in a part to be laser cut therefore cannot be neglected, and how they are negotiated often determines if a cut is deemed successful or not. Other geometrical effects include entry holes and sharp corners. Appropriate part-programming of the laser system can help to minimize their effect on quality degradation.

Because of the analytical difficulty in addressing such problems, not a great deal of work has been undertaken previously. It has been acknowledged though that only part of the incident beam power is available for laser cutting sheet metals [2]. This fraction was determined using a moving point source model. The model can be used to determine the interrelationship between cutting speed, cut width and power required for efficient laser cutting. Results are steady state values though, as it assumes a semi-infinite workpiece and constant cutting speed. Temporal variations of the available beam power should be considered. Experiments have been set up to investigate the transmission and reflection losses occurring through the laser interaction zone [3, 4]. These losses have been found to be greatest at slow processing speeds, where the beam centre can lie behind the cutting front [5].

Investigations into the cutting front mobility have also been carried out [6]. High speed photography of the cutting front showed it to be dynamic in nature. The formation of striations on the kerf edges is explained well by the relative motion of the front past the laser beam due to the exothermic reaction. The front then subsequently extinguishes, whereby re-initiation of the reaction occurs as the beam overtakes the front, and so the oscillation continues. It has been argued that power fluctuations can induce both temperature and molten layer thickness oscillations, thus causing striations to occur [7]. Such oscillations are indicative of the dynamic nature of the cutting front. A mono-dimensional finite difference model also clearly demonstrated that the front could possess mobility when cutting at constant processing speeds [8].

In this paper, a numerical model is developed in order to investigate the effect of various velocity profiles on the cutting front temperature. Inherent problems associated with a moving cutting front and temporal variations of the energy input per unit time (including not only transience in the absorbed beam power but also the exothermic

reaction energy) are resolved. These issues require a numerical approach, which would otherwise be impossible to address analytically.

2. THEORETICAL BACKGROUND

The starting point for any transient heat transfer analysis is the general heat conduction equation for an isotropic solid continuum. This suggests that for any such element, the net heat conducted in plus the heat generated within equals the elemental energy increase. If we assume constant thermo-physical properties and that the temperature distribution is homogeneous along the depth of the workpiece ($\partial T/\partial z = 0$, as can be assumed for the thin plate laser cutting case) then this reduces to the simpler 2D transient heat conduction equation of the form

$$\frac{K}{\rho c_v}\left(\frac{\partial^2 T}{\partial x^2} + \frac{\partial^2 T}{\partial y^2}\right) + \frac{\dot{q}}{\rho c_v} = \frac{\partial T}{\partial t}. \tag{1}$$

The initial temperature distribution at time $t = t_o$ is given as

$$T(x,y,t_o) = T_\infty(x,y),$$

where T_∞ is ambient room temperature. Naturally, boundary conditions must be specified at every boundary point. Often prescribed temperatures are given, but in practice this is clearly inappropriate. A much more acceptable boundary condition allows convection and radiation to occur to the surroundings with constant conditions h_c, h_r

$$-K_b \left.\frac{\partial T}{\partial n}\right|_b = (h_c + h_r)(T_b - T_\infty) \tag{2}$$

where n denotes the outward normal co-ordinate from the boundary and subscript b denotes a boundary point. In this situation, the boundary temperatures are not known until after the solution is determined.

The radiative heat transfer coefficient must be determined prior to the use of equation (2). This heat loss term is appropriately given by

$$q_r = \epsilon\sigma_b A(T_b^4 - T_\infty^4). \tag{3}$$

By definition:

$$q_r = h_r A(T_b - T_\infty). \tag{4}$$

Equating equations (3) and (4)

$$h_r = \epsilon\sigma_b(T_b + T_\infty)(T_b^2 + T_\infty^2). \tag{5}$$

Because of the fourth-power relationship in equation (3), radiation becomes dominant at high temperatures, as in the case of laser cutting. Although the workpiece temperature falls dramatically with increasing radial distance from the cutting zone, this heat transfer mechanism is included everywhere for the sake of completeness.

At all points other than where the oxygen gas jet impinges, it is assumed that there is no farfield streaming and thus natural or free convection occurs. However, underneath the cutting nozzle, forced convection is apparent and the resultant heat flux will generally be far greater than in the free convection case. Fully developed turbulent flow in a smooth tube is assumed for the forced convection case. In practice, supersonic flow is commonly encountered in CO_2 cutting, although turbulence within the kerf can be somewhat minimized by adjusting the nozzle-standoff distance. This allows cutting

to occur in a more stable zone. The Dittus–Boelter formula can be used to determine the Nusselt number [9].

$$Nu_d = 0.027\, Re_d^{0.8} Pr^{0.33} (\mu_m/\mu_w)^{0.14} \tag{6}$$

$$h_f = Nu_d K/d. \tag{7}$$

Although the free convection contribution is relatively small, it too is included for the sake of completeness. We can now express this situation in differential form.

$$\frac{K}{\rho c_v}\left(\frac{\partial^2 T}{\partial x^2} + \frac{\partial^2 T}{\partial y^2}\right) + \frac{\partial T}{\rho c_v \partial z}(h_f + h_n + 2h_r) + \frac{\dot{q}}{\rho c_v} = \frac{\partial T}{\partial t}. \tag{8}$$

Heat transfer to the substrate can be an important factor but we have assumed the use of a nail bed, honeycomb or mesh support, thus their conductive effect is small. Some reflections may occur in practice though, but free convection is simply assumed and radiation is considered both on the upper and lower surfaces.

The material removal process is in actual fact a rather complex interaction of the gas jet on the free surface of the melt, where shear stresses act on the cutting front and a boundary layer exists. It is assumed in our model that any area in the molten state is expelled out of the kerf immediately, by the force of the gas jet.

Let us also assume that the CO_2 laser source is of Gaussian TEM_{oo} mode. Its radial intensity distribution can then be given as

$$I(r) = I(0) \exp(-2r^2/R_b^2), \tag{9}$$

where $I(0)$ is the peak intensity, r is the radial distance from the beam centre, R_b is the laser beam radius at which point the power distribution falls to the industry accepted $1/e^2$ level.

Of the energy arriving at the cutting front, only a small percentage is absorbed. This is especially true when we consider depolarized or circularly polarized laser beams as is the case with co-ordinated motion laser cutting systems. Absorptivity values can be as low as 0.1, which is often limited by the oxide layer surface absorptivity about the cut face. The radial absorbed beam power is thus given as

$$P_b(r) = A_b I(r) = (1 - r_f) I(r), \tag{10}$$

where A_b is absorptivity and r_f is reflectivity.

The energy produced by the exothermic reaction cannot be neglected as its contribution is generally of the same order of magnitude as the absorbed laser beam power. It has been shown previously (through an ejected particle analysis) that approximately 50% of the melt ejected from the kerf is Fe and the remainder is almost completely FeO [10]. Assuming a pure oxygen supply for the assist gas, the following reaction occurs within the cutting kerf

$$Fe + 0.5\, O_2 = FeO \qquad \Delta H = -257.58\ \text{kJ/mol},$$

where ΔH is the energy released during the reaction and the ignition point is 1473.15 K [11].

If the mass removal rate of the melt out of the kerf is known or can be calculated, then the following relationship can be used to determine the energy obtained by reaction

$$P_{exo} = \text{ratio}\left(\frac{\dot{m}\Delta H}{\text{amu}}\right), \tag{11}$$

where amu = 1 mole FeO = 71.847 g/mol and ratio is the percentage of FeO:Fe ejected from the kerf.

This ratio is extremely sensitive to gas impurity levels, and the diffusion rate of O_2 into the melt is increased with increasing gas pressure. These factors make the prediction of this term difficult to establish in practice, whilst pressure variations are also common during cutting.

Because the material within the kerf is melted and then expelled, it is necessary to consider latent heat effects. In laser welding this is often neglected because the latent heat of fusion is compensated by the latent heat of solidification. In cutting though, the material is removed and as such only a very small liquid layer along the walls of the kerf can contribute to this heat of solidification.

$$P_{\text{melt}} = \dot{m} L_{\text{f}} \tag{12}$$

where $L_{\text{f}} = 275$ kJ/kg.

It has been assumed previously that the material removal rate can be given approximately by the following equation [12]

$$\dot{m} = \rho b D V_{\text{b}}. \tag{13}$$

This is only true though when it is assumed that the processing speed equals the front speed as in steady state cutting. In reality though, the front speed is the factor affecting the mass removal rate and not the cutting speed. The mass removal rate is therefore more appropriately given as

$$\dot{m} = \rho b D V_{\text{f}}. \tag{14}$$

V_{f} physically represents the solid–liquid interface speed, as all the molten material is assumed to be ejected out of the bottom of the kerf immediately. If the beam speed is too high, then melting and evaporation will cease. In this case, no melt ejection is possible and equations (13) and (14) are inappropriate. This condition is continually checked throughout programme execution and simulation ceases if it is violated.

Because kerf width fluctuations are generally small for high quality cutting, it is assumed that they are negligible and that the width is approximately of the same extent as that of the laser spot diameter. The kerf is therefore assumed to have a rectangular cross-section and the cutting front is assumed to be vertical. Such fluctuations have been considered elsewhere [13].

3. NUMERICAL MODEL

The determination of the mass removal rate is dependent upon firstly evaluating the cutting front speed.

From Fig. 2, it can be shown that

$$\Delta S_{\text{f}} = \Delta S_{\text{b}} - S + (S + \Delta S) = \Delta S_{\text{b}} + \Delta S. \tag{15}$$

In the time interval Δt, an expression for the front velocity can be ascertained

$$\frac{\Delta S_{\text{f}}}{\Delta t} = \frac{\Delta S_{\text{b}}}{\Delta t} + \frac{\Delta S}{\Delta t}. \tag{16}$$

The limit as $\Delta t \to 0$, yields the following instantaneous rates of change

$$\frac{\partial S_{\text{f}}}{\partial t} = \frac{\partial S_{\text{b}}}{\partial t} + \frac{\partial S}{\partial t}, \tag{17}$$

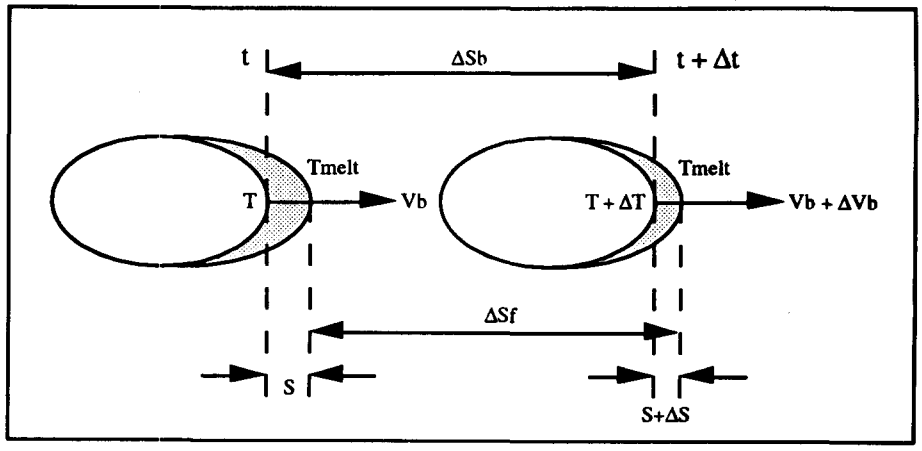

FIG. 2. Generation of cutting front mobility.

from which equation (17) can be expressed in the general form

$$V_f = V_b + \frac{\partial S}{\partial t}, \tag{18}$$

where $\frac{\partial S}{\partial t}$ is the time rate of change of the molten layer thickness.

The molten layer thickness is given by the shortest distance from the melting isotherm to the laser beam's centre at any given time t (see Fig. 2). The melting isotherm then represents the solid–liquid interface. A numerical expression for the average time rate of change of the molten layer thickness over the interval Δt can be obtained for evaluating the front velocity by using a method of first order interpolation between the nodal temperature T_m and the forward-shifted temperature T_{m+1}.

At time t = j

$$S^j = \Delta y \frac{(T_m^j - T_{melt})}{(T_m^j - T_{m+1}^j)}, \tag{19}$$

where m denotes the nodal point of interest in the y direction.

By analogy, at time $t + \Delta t$ = j + 1

$$S^{j+1} = \Delta y \frac{(T_m^{j+1} - T_{melt})}{(T_m^{j+1} - T_{m+1}^{j+1})} \tag{20}$$

from which

$$\frac{\Delta S}{\Delta t} = \frac{(S^{j+1} - S^j)}{\Delta t}. \tag{21}$$

In a time period Δt, the distance moved by the laser beam under either a net positive or negative acceleration a, relative to the workpiece is given by

$$\Delta S_b = V_b \Delta t + 0.5 a \Delta t^2. \tag{22}$$

In the first instance, because there is no acceleration or deceleration on the front, then the distance it has moved is simply given by

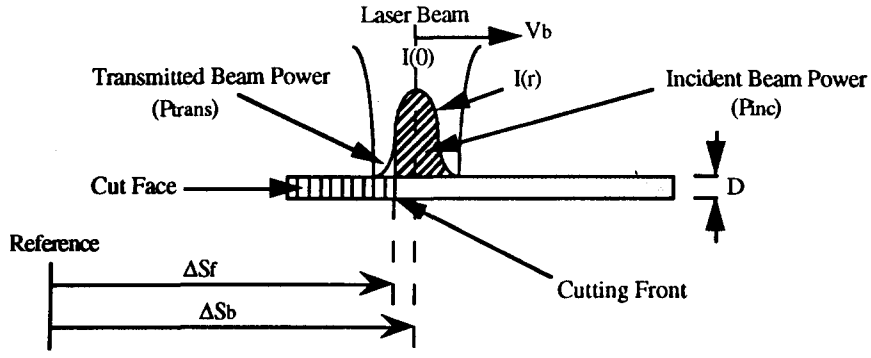

FIG. 3. Laser beam absorption and transmission losses in laser cutting.

$$\Delta S_f = V_f \Delta t. \tag{23}$$

The percentage of power incident on the workpiece is given by the proportion the cutting front is ahead of the trailing edge of the laser beam. If the front is behind the trailing edge of the laser beam, then all the beam power will fall on the workpiece and hence efficient beam coupling will be possible.

It cannot be simply assumed that the front will continue indefinitely at the current front speed. In fact, it will decrease if the beam decelerates because less beam power will now be available for processing. The opposite occurs under accelerating beam conditions. This means that the dynamics of the front regulates the proportion of energy lost through the kerf because the front quickly responds to the power gains and losses associated with various CNC velocity profiles (see Fig. 3).

4. COMPUTATIONAL ISSUES

Figure 4 shows the control volume of concern used in the modelling procedure. The workpiece is fixed in the cartesian plane whilst the laser beam is assumed to move relative to it.

Only half of the workpiece width is considered as the temperature distribution is

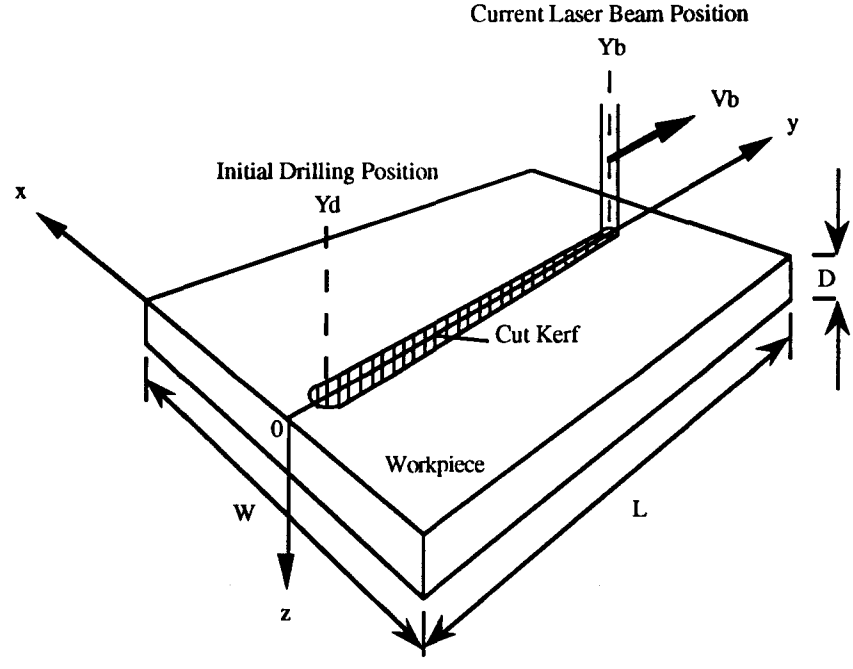

FIG. 4. Control volume and boundaries.

symmetrical about the OY axis. This eases computational effort and reduces the time requirement for solution. In doing so, the OY axis boundary in effect becomes an insulating surface, as no heat flux crosses it. Table 1 summarizes the model parameters used in the simulation and the thermo-physical properties assumed for mild steel.

After material is expelled from the kerf, conduction cannot occur across this region as these points are now part of the convective environment. The model accounts for this by removing all nodes above melting point which fall within the extent of the assist gas stream.

Heat diffusion equations are determined for all nodal points within the control volume and at boundaries. These balance equations can be solved in a number of ways. The explicit form is most appropriate for computer use and extremely fast. A numerical stability condition limits the timestep of integration Δt, so that divergent oscillations of the calculated temperatures are avoided. This condition makes it impossible to study various CNC acceleration and deceleration curves and thus the implicit method was used. The implicit method has unlimited numerical stability but is more difficult to solve as a set of simultaneous equations ensues. The Gauss–Seidel iteration method was used to solve these. All nodes were swept by their appropriate equations until the temperatures converged to some previously set limit. For example, in the case where an appropriate initial temperature distribution is required prior to cutting, equation (24) calculates the new nodal temperature at time j + 1

Condition: $\{X = 0 \text{ and } 0 < (Y = Y_d) < L\}$ and assist gas = air

$$T_{m,n}^{j+1} = \frac{T_{m,n}^{j} + \sigma\left[\frac{H}{KD} + T_{m-1,n}^{j+1} + T_{m+1,n}^{j+1} + 2T_{m,n+1}^{j+1} + Bi_f\frac{T_\infty \Delta y}{D} + Bi_n\frac{T_\infty \Delta y}{D} + 2Bi_r\frac{T_\infty \Delta y}{D}\right]}{\left(1 + 4\sigma + \sigma Bi_f\frac{\Delta y}{D} + \sigma Bi_n\frac{\Delta y}{D} + 2\sigma Bi_r\frac{\Delta y}{D}\right)}, \tag{24}$$

where

$$H = P_b(0) - P_{melt} \tag{25}$$

$$\sigma = \frac{\alpha \Delta t}{\Delta y^2} \tag{26}$$

$$Bi_f = \frac{h_f \Delta y}{K}, \quad Bi_n = \frac{h_n \Delta y}{K}, \quad Bi_r = \frac{h_r \Delta y}{K}. \tag{27}$$

With cutting underway, the above equation is corrupted to the following form because of the existence of the kerf

TABLE 1. EXPERIMENTAL FRAME

Model parameters and physical quantities	
Gaussian TEM_{00} CO_2	amu = 71.847 g/mol
5″ focal lens	σ_b = 5.67E − 8 W/m² K⁴
R_b = 250 μm	L_f = 275 kJ/kg
A_b = 0.4	T_{melt} = 1809.15 K
K = 51 W/m K	T_∞ = 293.15 K
α = 1E − 5 m²/s	ρ = 7865 kg/m³
ΔH = − 257.58 kJ/mol	$\Delta x = \Delta y$ = 125 μm

Condition: $\{X = 0 \text{ and } 0 < (Y = Y_b) < L\}$ and assist gas = oxygen

$$T_{m,n}^{j+1} = \frac{T_{m,n} + \sigma\left[\frac{H}{KD} + T_{m+1,n}^{j+1} + 2T_{m,n+1}^{j+1} + Bi_f T_\infty + Bi_f \frac{T_\infty \Delta y}{D} + Bi_n \frac{T_\infty \Delta y}{D} + 2Bi_r \frac{T_\infty \Delta y}{D}\right]}{\left(1 + 3\sigma + \sigma Bi_f + \sigma Bi_f \frac{\Delta y}{D} + 2\sigma Bi_r \frac{\Delta y}{D} + \sigma Bi_n \frac{\Delta y}{D}\right)}, \tag{28}$$

where

$$H = P_b(0) + P_{exo} - P_{melt}. \tag{29}$$

Once all the discretized equations have converged, the model determines the current front velocity, from which the exothermic power is calculated using this value. The percentage of transmitted power lost through the kerf is then evaluated. The status of the current laser beam position relative to the workpiece is updated and a new timestep of integration is obtained. The model then loops and the procedure repeated until the laser beam reaches its user-specified final stopping position, or until front temperatures fall below melting point. This indicates that cutting conditions are poor and that quality can no longer be assured.

5. DISCUSSION OF RESULTS

Results are presented in the order of how a cut would normally be performed in practice. This sequence starts with cut initiation issues and ends with either cut termination to a boundary edge or deceleration to a specific point within the workpiece.

5.1. *Cut initiation*

On most occasions, it is necessary to initiate a keyhold in the work material prior to cutting. This issue is considered so that a realistic initial temperature distribution can be obtained before cutting simulation commences. Two basic methods can be employed to produce such a hole. The first is by pulsing the laser with an assist gas. This method generally takes a fair amount of time but produces neat starting holes. The second method commonly used is called blast drilling. It uses continuous wave beam power with an assist gas to blow the melted material away. In both methods, molten material can only be ejected upwards in all directions until complete penetration. The second method creates a hole very quickly, but these are generally of larger size than the first method. Keyholes are often larger than the kerf widths produced when cutting because of the localized overheating that occurs in these regions.

It is apparent that the extra power supplied by the rather explosive reaction means that the temperature gradients obtained for the oxygen case will be steeper than those possible for the air-assisted case. This is because of the shorter diffusion time associated with reactive gas drilling. It was noted that under identical simulation conditions, it took only 2.2 ms for the temperature in the workpiece to reach the melting point (and thus form an initiation hole) in the oxygen-assisted case, as compared with 38 ms for the air-assisted case.

These times represent minimum drilling times, and it is obvious that drilling periods greater than these will result in practice. To obtain more realistic penetration times, it is necessary to consider the temperature distribution along the depth of the workpiece, and to consider other effects such as the formation of surface plasma [14]. Once a kerf is formed, the effect of these plasmas is reduced somewhat due to the ability of the gas jet to remove it more effectively. Surface plasmas are neglected in this model as the main emphasis is for simulating the cutting process as opposed to the drilling

one. Drilling the initiation hole for longer than is necessary can cause the workpiece to overheat in the region about this point. This may cause degradation of quality when cutting commences. It has been suggested that cooling these blast holes prior to cutting allows the workpiece temperature to fall sufficiently so that uncontrollable burning is avoided.

5.2. *Actuator acceleration limits*

The next stage in the cutting sequence involves command generation which will allow the cutting action to commence. Large axis inertias and torque limitations must be considered as precise control of axis acceleration, velocity and position are essential for successful command generation.

Let us consider velocity profiles necessary in order to accelerate actuators up to their desired speeds, so that torque limits are not exceeded.

Figure 5(a) shows the responses of the cutting front to various accelerations for reactive gas cutting. A target velocity of 33 mm/s is desired from all three velocity profiles. In the slow acceleration case, the front velocity lags behind the beam velocity but closely follows it and smoothly approaches the target speed. As the accelerations increase in size, it is evident that the front begins to possess oscillatory characteristics. The cutting front velocities clearly overshoot their target initially but ultimately decay in a stable fashion. The results are supported by a numerical investigation undertaken previously [8].

Figure 5(b) shows the corresponding cutting front temperatures obtained for the various initial ramp accelerations. Similar results were found experimentally for cuts produced in aluminium workpieces [15]. If the accelerations become too large (i.e. 2.178 m/s^2), the effect on the front is such that the temperature falls below the melting point and thus cutting becomes impossible. This is because the diffusion time is not substantial enough as the beam is traversing so quickly that the rate of energy deposition is insufficient to cause workpiece melting.

It can be seen that under the accelerations imposed, all the front temperatures gradually approach a common steady state value. This translates into a distance of approximately 2.5 mm after the blast hole where transience is present. This unstable zone will generally be accommodated with at least some form of varying quality,

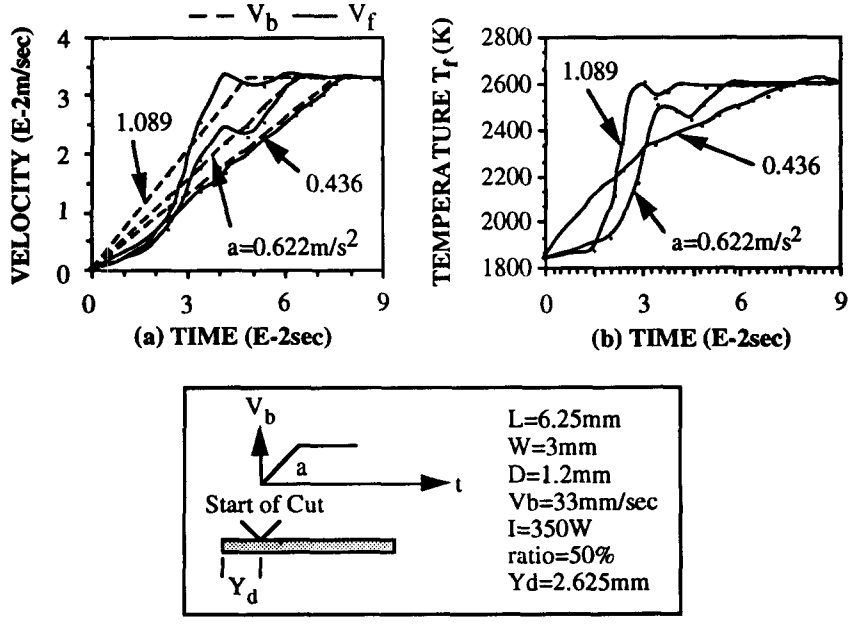

FIG. 5. Effect of various actuator accelerations on (a) the cutting front velocity and (b) the cutting front temperature.

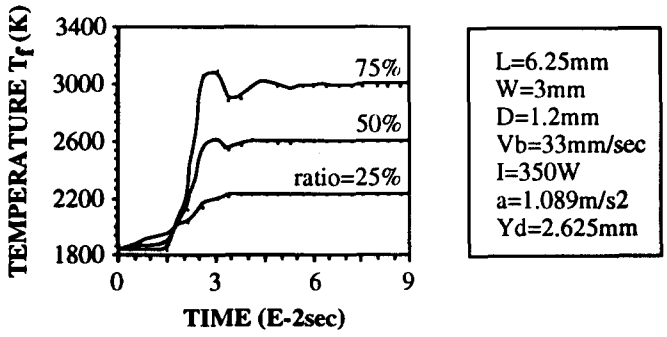

FIG. 6. Effect of the contribution of exothermic power on the cutting front temperature.

be it material overheating, uncontrolled burning, kerf widening or excessive surface roughness.

Figure 6 demonstrates the effect of various amounts of exothermic power on the resulting cutting front temperature. An oscillation becomes apparent and increases in magnitude as its contribution increases. Figure 5(a) showed that cutting front oscillations were visible under certain conditions. Because the exothermic power depends on the front velocity (refer to equations (11) and (14)), then any oscillation associated with the front will result in an oscillation of this energy input. Under significant contributions then, temporal variations of this power term can translate into a temperature fluctuation.

5.3. *Steady state conditions*

As mentioned previously, if sufficient time elapses (under certain conditions), then steady state can be reached. Once steady state has been reached, the temperature will be maintained until a boundary is encroached upon. Uncontrollable factors such as rust, scale and material imperfections may cause some imbalance. Figure 7(a) shows that with speed increases, the cutting front temperature also increases. Others have validated this trend experimentally under different cutting conditions [6]. It is expected that with further speed increases, the front temperature will continue to increase up to and beyond the vaporization point, resulting in significant evaporation effects.

Figure 7(b) shows that as the cutting speed increases, more efficient cutting occurs because of the greater beam coupling to the work material. This is expressed as a drop in the level of transmitted power falling straight through the kerf with no effect. High

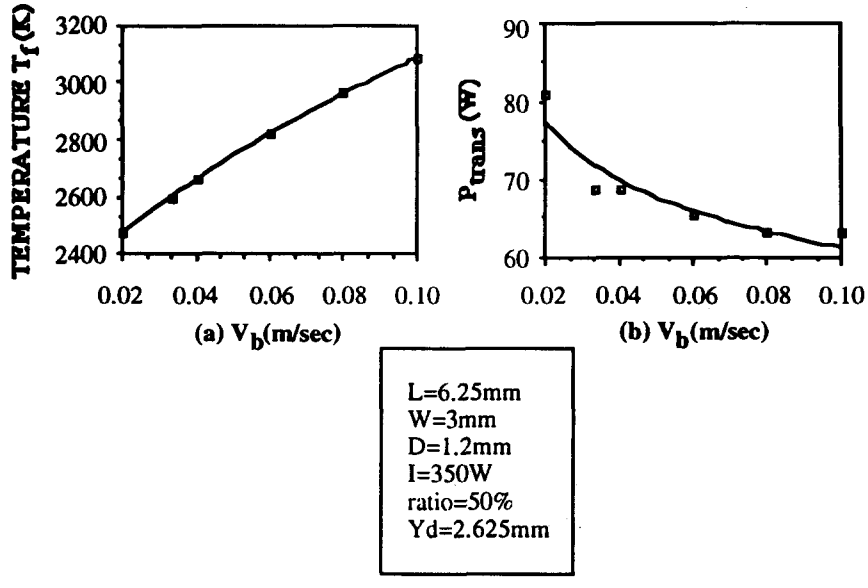

FIG. 7. Effect of cutting speed on (a) the cutting front temperature and (b) the transmitted power.

processing rates therefore not only aid productivity levels but also improve the efficiency of the overall laser cutting process.

5.4. *Boundary encroachment*

Figure 8(a) shows that although the cutting speed remains constant right up to the workpiece edge, the front velocity begins to deviate over the last 1 mm or so. This is because heat diffusion is more difficult at such boundaries.

Because the front velocity gradually increases, the amount of beam coupling to the workpiece falls significantly. Figure 8(b) shows the amount of transmitted power falling straight through the kerf with no effect increases on boundary approach. If this effect is not accounted for and as such temporal beam coupling issues are neglected, then the temperature rise observable in Fig. 8(c) would be considerably steeper than it is as a result. Similar temperature trends for such a boundary encroachment were found experimentally [15].

Figure 9 shows the resulting temperature contour plots of the cutting process at particular laser beam positions under the same conditions as Fig. 8. The isotherms clearly change both in shape and size as time progresses because the model considers multidimensional unsteady heat conduction. Note that the presence of the kerf along the centre of the workpiece makes the isotherms deviate from the classical "egg"-shaped isotherms that are well known for moving sources of heat.

5.5. *An optimization strategy via actuator deceleration*

Figure 8(c) showed that quality cannot be assured right up to workpiece edges because of the temperature rise associated with the encroachment. An optimization strategy that could force the cutting front temperature to remain a constant to the boundary, and thus maintain quality of cut, would be of considerable value.

Since speed increases can effectively improve beam coupling and result in cutting front temperature increases, by analogy, a deceleration profile must exist which can result in the front temperature remaining at its steady state value for all subsequent

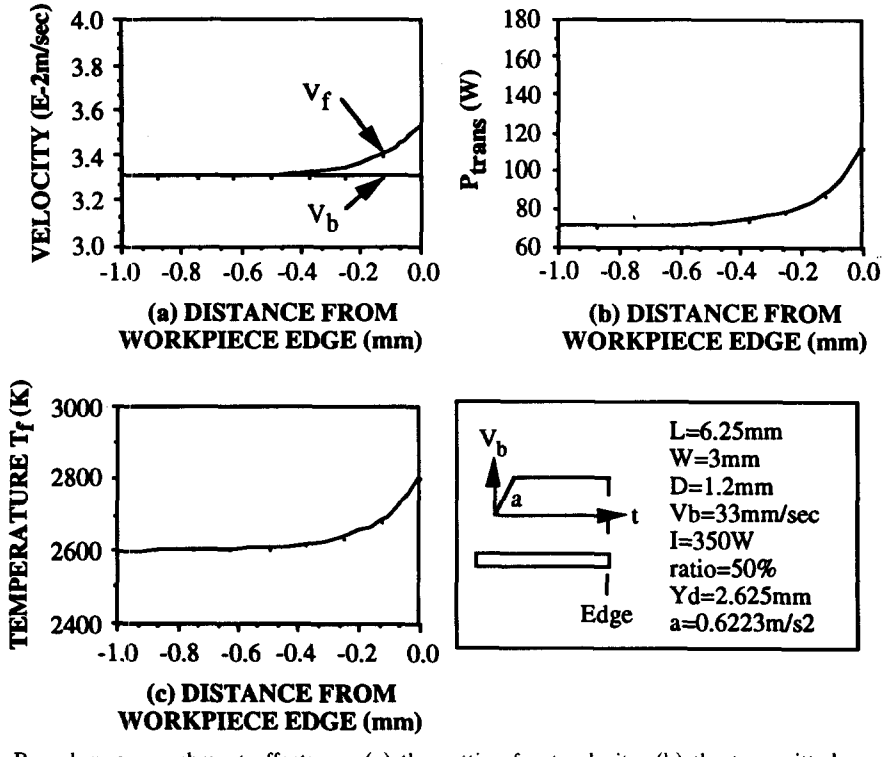

FIG. 8. Boundary encroachment effects on: (a) the cutting front velocity; (b) the transmitted power; and (c) the cutting front temperature.

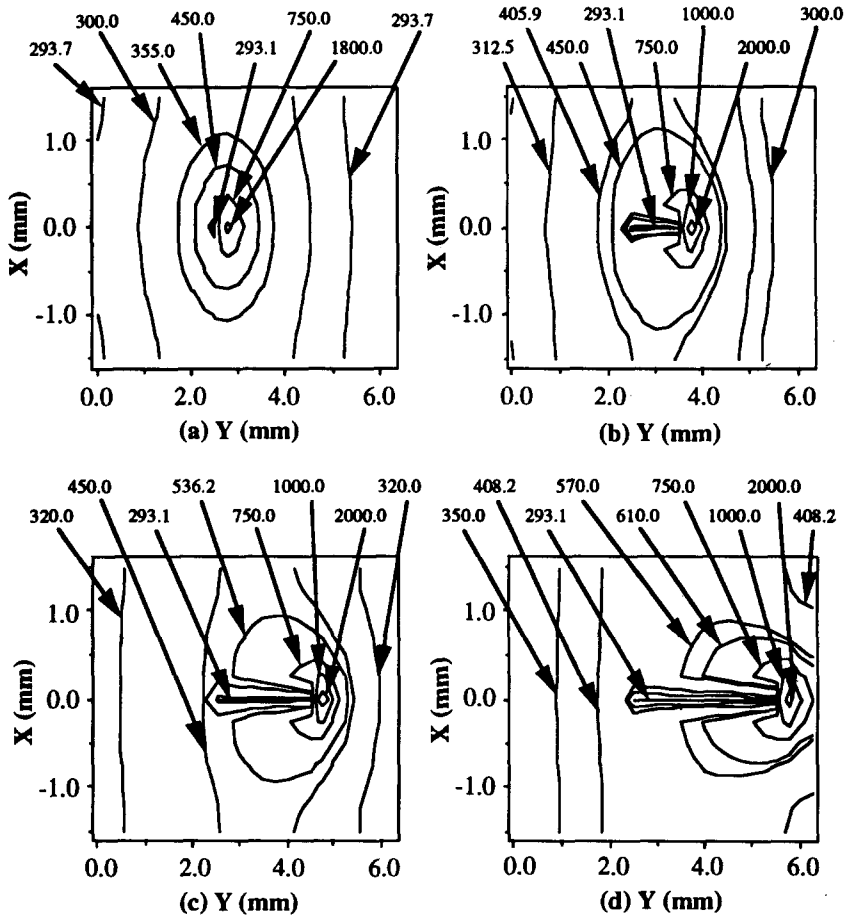

FIG. 9. Contour plots of the temperature distribution generated (K) at particular laser beam positions: (a) Y_b = 2.875 mm; (b) Y_b = 3.875 mm; (c) Y_b =4.875 mm; and (d) Y_b = 5.875 mm. Cutting conditions as per Fig. 8.

instances in time. The problem is therefore one of minimizing the deviation from steady state. It is expected that only a non-linear velocity profile could optimize such a task as the interrelationships are complex.

The strategy developed is iterative by nature and is conceptually summarized in Fig. 10. The model proceeds forward in time by the accumulation of the timestep Δt of

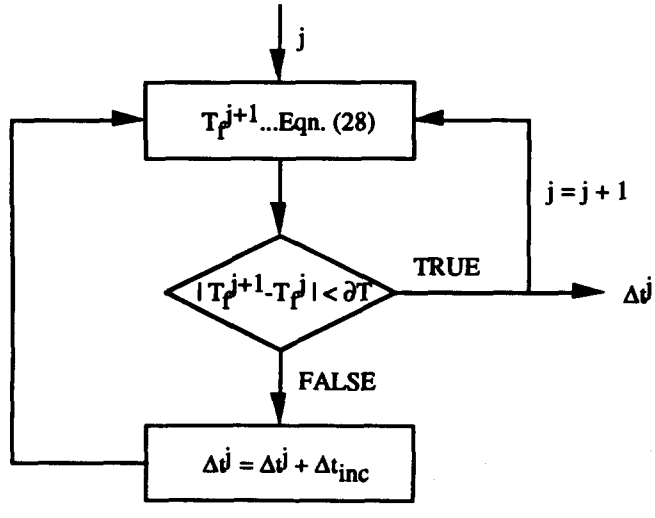

FIG. 10. Optimization strategy for velocity profile determination.

integration. By monitoring the front temperature at every instance, a steady state value can be established, that is

$$|T_f^{j+1} - T_f^j| < \partial T. \tag{30}$$

If the cutting speed remains constant, this steady state value can only be disturbed subsequently by a boundary encroachment. As the change in the temperature exceeds the previously set limit ∂T, a course of action is required to minimize this deviation. By taking advantage of the fact that the model proceeds forward in time, an increase in the timestep by a very small interval Δt_{inc} is effectively a slight deceleration in speed from its previous value as the spatial increments are unchanged.

$$\Delta t = \Delta t + \Delta t_{inc}. \tag{31}$$

This new timestep is used to obtain an updated mesh Fourier number so that equation (28) can be solved for T_f^{j+1}. If the temperature is still unacceptable, the timestep is increased further and the procedure repeated, until the temperature is stabilized.

With the standard bisection method, iteration steps are halved when the procedure overshoots the target value so that an improved solution is obtainable. Because the timesteps chosen are very small, this is not required so that the model only steps forward in time. Previous values therefore need not be remembered, resulting in a more efficient and improved solution rate.

The next beam position is likely to generate a front temperature outside the set bounds, and thus the strategy must be repeated again, until all values of temperature are acceptable right up to the workpiece edge.

Figure 11(c) shows the results obtained using the optimization strategy. Clearly the cutting front temperature has been stabilized. The generated cutting speed V_b is non-linear and needs to become very steep in the final stages in order to maintain the front

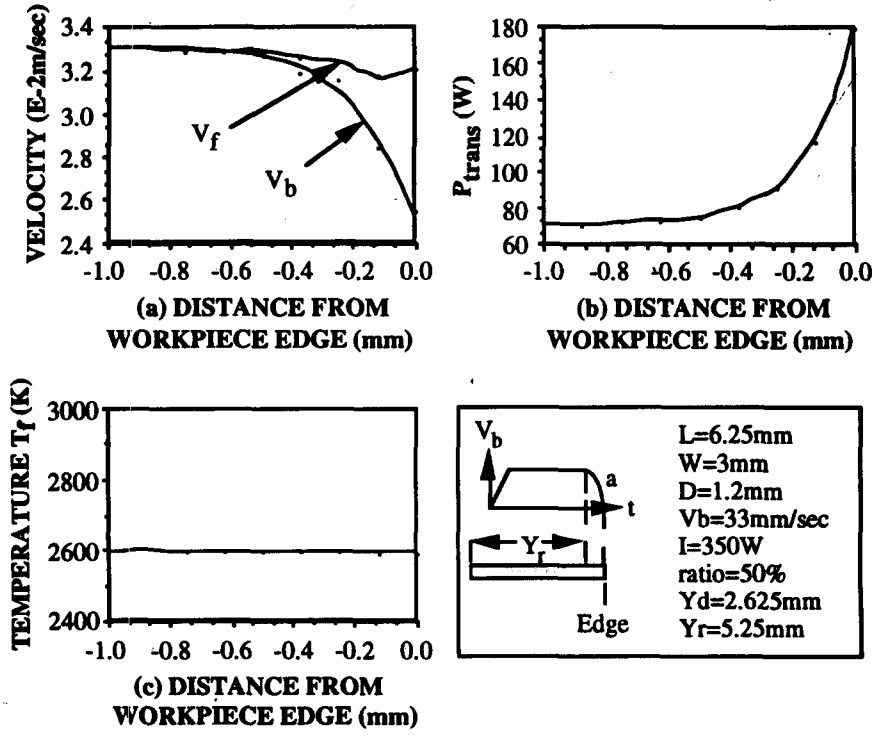

FIG. 11. Effect of the optimized velocity profile on: (a) the cutting front velocity; (b) the transmitted power; and (c) the cutting front temperature.

temperature at a constant. The front velocity initially follows the cutting speed but then deviates substantially on approach to the boundary. Refer to Fig. 11(a). Figure 11(b) also shows that transmission losses need to become excessive in order to stabilize the front temperature.

6. CONCLUSIONS

The numerical model developed examined various CNC velocity profiles for their effect on the resulting cutting front temperature. As such, issues such as cutting front mobility and temporal beam coupling effects are resolved. The presence of the kerf was considered and became part of the convective environment. This made diffusion more difficult and forced the front temperature higher than would be expected from well behaved analytical models (which simplistically allow conduction to occur across such boundaries). Results clearly showed that accelerations caused greater, more efficient beam coupling. The implication of actuator retardation was shown to result in a reduction in the amount of beam coupling and hence an associated temperature drop was evident. Larger exothermic power contributions were shown to cause oscillatory behaviour in the temperature not evident at smaller values. The dynamics of the cutting front was found to respond quickly to typical velocity profiles and stable decay to the target speed was always found. Steady state cutting front temperatures were also found to increase with increasing cutting speed. Boundary encroachment and bulk heating effects (due to workpiece geometry) caused the front velocity to increase dramatically on approach to a workpiece edge, so that even without a processing speed change, beam coupling was significantly reduced as a result. A non-linear velocity profile was evaluated via an optimization strategy which stabilized the cutting front temperature to its steady state value. As such, quality can therefore be assured for laser cutting workpieces right up to pre-cut sections and boundaries. Results on front mobility and temperature show similar trends as experimental and numerical results found elsewhere, whilst their direct verification is currently under investigation. Due to the hostile environment encountered in the interaction zone, the observation of such phenomena is extremely difficult.

Acknowledgements—The authors gratefully acknowledge the support given by the Australian Research Council and the School of Mechanical and Manufacturing Engineering, The University of New South Wales, Australia. Valuable discussions with Prof. M. Behnia are also duly acknowledged.

REFERENCES

[1] P. Di Pietro and Y. L. Yao, An investigation into characterizing and optimizing laser cutting quality—a review, *Int. J. Machine Tools Manufact.* **34** (2), 225–243 (1994).
[2] J. N. Gonsalves and W. W. Duley, Cutting thin metal sheets with the CW CO_2 laser, *J. Appl. Phys.* **43** (11), 4684–4687 (1972).
[3] J. Powell, *CO_2 Laser Cutting*, pp. 218–222. Springer, London (1993).
[4] I. Miyamoto *et al.*, Beam Absorption Mechanism in Laser Welding, in Laser Processing: Fundamentals, Applications, and Systems Engineering, SPIE **668**, 11–18 (1986).
[5] U. Schreiner-Mohr *et al.*, New aspects of cutting with CO_2-lasers, ICALEO, SPIE **1722**, 263–272 (1991).
[6] Y. Arata *et al.*, Dynamic behaviour in laser gas cutting of mild steel, *Trans. JWRI* **8** (2), 15–26 (1979).
[7] D. Schuocker, Dynamic phenomena in laser cutting and cut quality, *J. Appl. Phys. B* **40**, 9–14 (1986).
[8] S. F. Yuan *et al.*, Thermical modelisation of laser cutting process, Laser Technologies in Industry, SPIE **952**, 583–591 (1988).
[9] F. M. White, *Heat and Mass Transfer*, pp. 332–336. Addison-Wesley, Reading, MA (1988).
[10] J. Powell *et al.*, The role of oxygen purity in laser cutting of mild steel, pp. 1–10. *ICALEO*, Florida, U.S.A. (1992).
[11] M. Geiger *et al.*, Laser cutting of steel sheets, Laser Assisted Processing, SPIE **1022**, 20–33 (1988).
[12] D. Schuocker, Heat conduction and mass transfer in laser cutting, Laser Technologies in Industry, SPIE **952**, 592–599 (1988).
[13] P. Di Pietro and Y. L. Yao, A new technique to characterize and predict laser cut striations, Prosperity Through Competitive Manufacturing, *Proc. of Australian Conf. on Mfg Engng* (ACME '93), pp. 327–333. Adelaide, Australia, 22–24 November (1993).
[14] B. S. Yilbas *et al.*, Study into the measurement and prediction of penetration time during CO_2 laser cutting process, *J. Engng Manufact.* **204**, 105–113 (1990).
[15] M. Hansmann *et al.*, Influence of workpiece temperature in laser cutting, *Laser Treatment of Materials* (edited by B. L. Mordike), pp. 309–317. DGM Informationsgesellschaft mbH, Germany (1987).